Chapter 4

GENERALISED HUMAN SENSORY NERVE FIBRE MODEL

Smit, J. E., Hanekom, T. and Hanekom, J. J. (2008) Modelled temperature-dependent excitability behaviour of a generalised human peripheral sensory nerve fibre, *in review*

4.1 INTRODUCTION

This chapter deals with the second phase in the development of the ANF model, namely the development of the generalised human peripheral sensory nerve fibre model, based on a combination of the models by Rattay *et al.* (2001b) and Blight (1985) and constructed using human sensory nerve fibre morphometric data. Ranvier node dynamics utilised the Ranvier node model described in Chapter 3. However, Bostock and Rothwell (1997) included a persistent sodium current in addition to the transient sodium current, as modelled in Chapter 3, and was therefore able to better explain chronaxie times compared to a model that only included the transient sodium current. Therefore the sensory nerve fibre model described in this chapter included this additional persistent sodium current.

The objective of this chapter is to determine if the human Ranvier node model, which is

based on a modified version of the HH model, together with the additional persistent sodium current can predict the excitability behaviour in human peripheral sensory nerve fibres with diameters ranging from 5.0 – 15.0 μm. The Ranvier node model is extended to include a persistent sodium current and is incorporated into a generalised simple double-cable nerve fibre model. Parameter temperature dependence is included.

4.2 MODEL AND METHODS

4.2.1 Parameters applied to the nerve fibre model

Rattay *et al.* (2001b) developed a nerve fibre cable model which assumes a propagating action potential driven by Hodgkin-Huxley (Hodgkin and Huxley, 1952) dynamics. The model consists of dendritic, somal and axonal sections. The dendritic and axonal sections are divided into cylindrical compartments, with alternative compartments representing unmyelinated Ranvier nodes and myelinated internodes. Membrane potential (V_n) change at the centre of the nth compartment is described by the cable equation

$$C_{m,n}\frac{(V_n)}{dt} = \left[-I_{ion,n} + \frac{(V_{n-1}+V_{e,n-1})-(V_n+V_{e,n})}{R_{n-1}/2+R_n/2} + \frac{(V_{n+1}+V_{e,n+1})-(V_n+V_{e,n})}{R_{n+1}/2+R_n/2}\right], \tag{4.1}$$

with V_n offset by the resting membrane potential (V_{res}) and having an initial value $V_n(0)$ equal to zero. $C_{m,n}$ is the membrane capacitance and R_n the axoplasmic resistance to the neighbouring sections at the nth compartment.

The proposed human nerve fibre model was based on the Rattay model, but consisted of an axonal section only (Figure 4.1). The modelled nerve fibre was externally stimulated with a monopolar electrode positioned sufficiently far away so that the propagating action potential was minimally distorted by the external potential field (V_e). The Ranvier nodes were considered unmyelinated active axolemmae utilising the new human Ranvier node model dynamics described in Chapter 3. For completeness the human nodal model equations will be given here, together with model parameter values (Tables 4.1 and 4.2), but for a more comprehensive description please refer.

In myelinated nerve fibres the total nodal sodium current (I_{Na}) is subdivided into

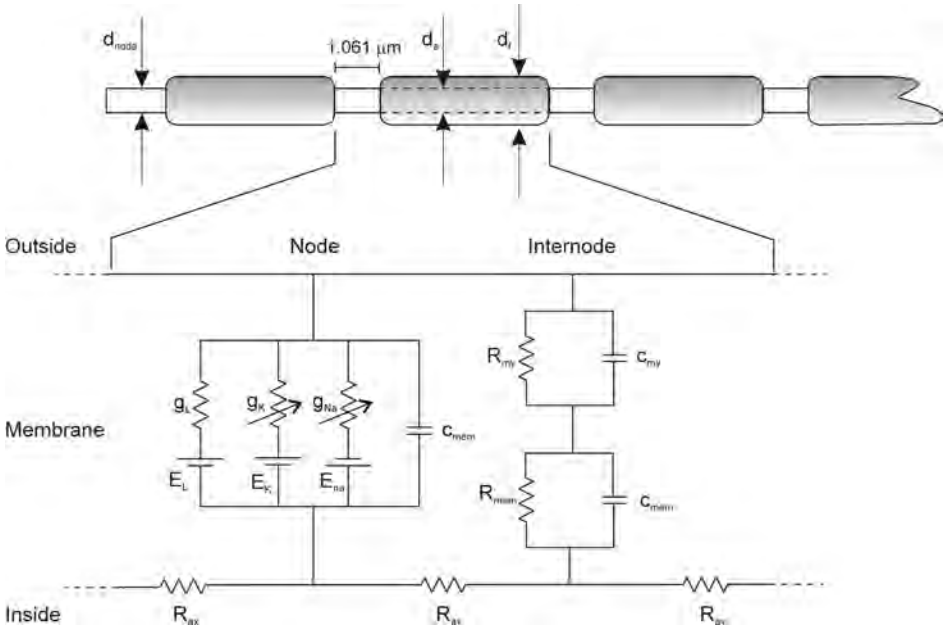

Figure 4.1: Representation of the generalised human peripheral sensory nerve fibre. The cable model consisted of a myelinated axon with 23 nodes separated by 22 internodes. Each node had a length of 1.061 μm and diameter d_{node}. The internodal axolemmal diameter (d_a) and internodal length depended on the total internodal nerve fibre diameter (d_f). The myelinated internodes were considered to be simple double cable structures as modelled by Blight (1985). In the equivalent circuit diagram the resistances and capacitances of the leaky myelin sheath (R_{my}, c_{my}) and axolemma (R_{mem}, c_{mem}) were combined together in series to form one compartment. The axoplasmic resistance (R_{ax}) was a function of the axoplasmic resistivity. The nodal circuit consisted of the axolemmal (membrane) resistance (R_{mem}) and capacitance (c_{mem}), as well as expressions for the sodium (g_{Na}), potassium (g_K) and leakage (g_L) conductances and equilibrium potentials (E_{Na}, E_K, E_L). The total nodal sodium current (I_{Na}) was subdivided into a 2.5% persistent (I_{Nap}) and 97.5% transient (I_{Nat}) sodium currents.

two functionally distinct currents. The transient sodium (I_{Nat}) current constitutes the largest proportion ($\sim$ 98%) and has fast activating and inactivating kinetics. A smaller current ($\sim$ 2%) activates equally fast, but at membrane potentials 10 – 20 mV more negative than the transient, and inactivates slowly or not at all; forming a persistent (I_{Nap}) current (Burke, Kiernan and Bostock, 2001). Schwarz *et al.* (1995) developed a human Ranvier node model including only I_{Nat}. Bostock and Rothwell (1997) developed a similar model to the one by Schwarz *et al.* (1995) and estimated chronaxie times of 176 μs at skin temperature. When the model was changed to include a 2.5% I_{Nap} activated at 10 – 20 mV more negative than I_{Nat} and the sodium activation slowed by a factor 2, the chronaxie time increased to 535 μs. The present human nerve fibre model therefore included a 2.5% I_{Nap} in addition to a 97.5% I_{Nat}.

The persistent current was set to activate at 20 mV more negative than the transient current and the sodium activation was slowed down.

The ionic membrane currents in the present human nerve fibre model could therefore be described in terms of temperature-dependent sodium (g_{Na}), potassium (g_K) and leakage (g_L) ionic conductances, as well as ionic equilibrium potentials

$$\begin{aligned} I_{ion}(T) = {} & 0.975 g_{Na}^{max}(T)\, m_t^3 h\,(V - V_{Na}(T)) + g_K^{max}(T)\, n^4\,(V - V_K(T)) \\ & + 0.025 g_{Na}^{max}(T)\, m_p^3 h\,(V - V_{Na}(T)) + g_L(T)\,(V - V_L(T)) \qquad \left[\mu A/cm^2\right]. \end{aligned} \tag{4.2}$$

Ionic currents are considered ohmic and are given in terms of the ionic conductances and change in membrane potential. Ion channel activation and inactivation probability dynamics (m_t, m_p, h and n respectively) were described by

$$\frac{dx}{dt} = \alpha_x(V)\,[1 - x] - \beta_x(V)\,x, \quad x = m, n, h \tag{4.3}$$

with initial values $m_t(0) = m_p(0) = 0.5$, $h(0) = 0.6$, $n(0) = 0.32$, and given in terms of the voltage-dependent opening and closing rates of the ion channels $\alpha(V)$ and $\beta(V)$

$$\alpha_{mt}, \alpha_{ns} = AQ_{10}^{(T-T_0)/10} \cdot \frac{B - CV}{D\,(\exp(B - CV)) - 1} \qquad [m/s], \tag{4.4a}$$

$$\beta_{mt}, \beta_{ns}, \alpha_h = AQ_{10}^{(T-T_0)/10} \cdot B \exp\left(\frac{-V}{C}\right) \qquad [m/s], \tag{4.4b}$$

$$\beta_h = AQ_{10}^{(T-T_0)/10} \cdot \frac{1}{(1 + \exp(B - CV))} \qquad [m/s], \tag{4.4c}$$

$$\alpha_{mp} = AQ_{10}^{(T-T_0)/10} \cdot \frac{B - C(V - \Delta V)}{D\,(\exp(B - C(V - \Delta V))) - 1} \qquad [m/s], \tag{4.4d}$$

$$\beta_{mp} = AQ_{10}^{(T-T_0)/10} \cdot B \exp\left(\frac{-(V - \Delta V)}{C}\right) \qquad [m/s], \tag{4.4e}$$

where ΔV indicates that the persistent sodium current activated 20 mV more negative than the transient sodium current. Acceleration of the activation and inactivation of the membrane's permeability to specific ion species, as suggested by Huxley (1959), is given by parameter **A** values (Table 4.1). In accordance with Bostock and Rothwell (1997), activation of the sodium permeability of I_{Nap} was slowed down by a factor 2.2. Parameters **B**, **C** and **D** are the original HH model parameters, which are considered constant (Hodgkin and Huxley, 1952).

Table 4.1: Parameters used for calculation of the voltage-dependent opening and closing rates of the ion channels. The transient sodium current activation parameters are subscripted with a t and the persistent sodium current activation parameters by a p.

Parameter	**Q_{10}**	**T_0 (°C)**	**A**	**B**	**C**	**D**
α_{mt}	2.16	20	4.42	2.5	0.1	1
β_{mt}	2.16	20	4.42	4.0	18	–
α_h	1.5	20	1.47	0.07	20	–
β_h	1.5	20	1.47	3.0	0.1	–
α_{ns}	1.5	20	0.20	1.0	0.1	10
β_{ns}	1.5	20	0.20	0.125	80	–
α_{mp}	1.99	20	2.06	2.5	0.1	1
β_{mp}	1.99	20	2.06	4.0	18	–

The equilibrium potentials were given in terms of the Nernst potential equations for the different ion species (Hille, 2001)

$$V_{Na}, V_K, V_L = \frac{1000RT_K}{F} \ln\left(\frac{[ion]_o}{[ion]_i}\right) - V_{rest} \qquad [mV]\,, \tag{4.5}$$

with R the universal gas constant, F the Faraday constant, T_K the absolute temperature (in Kelvin) and $[ion]_o/[ion]_i$ the extracellular to intracellular ion concentration ratio for Na^+, K^+ and leakage ions respectively (Table 4.2).

In an additional modification to the original Rattay cable model the myelinated internodes were considered to be simple double cable structures as modelled by Blight (1985). The leaky myelin sheath and axolemma were combined together in series, having high resistance and low capacitance. The internodal capacitance (c_{int}) was given by

$$c_{int} = \left(\frac{1}{c_{mem}} + \frac{N_{my}}{c_{my}}\right)^{-1} \qquad \left[\mu F/cm^2\right], \tag{4.6}$$

with c_{mem} the same value as the nodal membrane capacitance and c_{my} the myelin membrane capacitance (Table 4.2). The number of myelin layers (N_{my}) was given by

$$N_{my} = \lfloor 0.5\,(d_f - d_a)\rfloor / l_{my}, \tag{4.7}$$

with d_f the total internodal nerve fibre diameter (cm), d_a the internodal axolemmal diameter (cm) and l_{my} the myelin layer thickness equal to 0.016 μm (Blight, 1985).

Table 4.2: Model electrical parameters.

Parameter	**Value**	**Q_{10}**	**T_0 (°C)**	**Reference**
Membrane resting potential (V_{rest})	-79.4 mV	1.0356 (T $\leq$ 20 °C) 1.0345 (T > 20 °C)	6.3	Hodgkin and Huxley (1952), Schwarz *et al.* (1995), Wesselink *et al.* (1999) †
Gas constant (R)	8.3145 J/K.mol			Atkins (1995)
Faraday constant (F)	9.6485×10^4 C/mol			Atkins (1995)
$[Na^+]_o/[Na^+]_i$	7.2102			Hodgkin and Huxley (1952), Schwarz *et al.* (1995), Wesselink *et al.* (1999), Hille (2001) #
$[K^+]_o/[K^+]_i$	0.0361			Reid *et al.* (1993), Scholz *et al.* (1993), Schwarz *et al.* (1995)
$[Leakage]_o/[Leakage]_i$	0.036645			Scholz *et al.* (1993), Schwarz *et al.* (1995) ††
Na^+ conductance (g_{Na})	640.00 mS/cm^2	1.1	24	Scholz *et al.* (1993), Hille (2001)
K^+ conductance (g_K)	60.0 mS/cm^2	1.16	20	Reid *et al.* (1993), Scholz *et al.* (1993), Schwarz *et al.* (1995) ††
Leakage conductance (g_L)	57.5 mS/cm^2	1.418	24	Schwarz and Eikhof (1987), Scholz *et al.* (1993), Schwarz *et al.* (1995) ††
Axoplasmic resistivity (ρ_{ax})	0.025 kΩ.cm	$(1.35)^{-1}$	37	Wesselink *et al.* (1999) †
Membrane capacitance (c_{mem})	2.8 μF/cm^2			Schwarz *et al.* (1995) *
Myelin membrane capacitance (c_{my})	0.6 μF/cm^2			Blight (1985)
Membrane resistance (R_{mem})	4.8707×10^4 Ω.cm^2	$(1.3)^{-1}$	25	Blight (1985) †
Myelin membrane resistance (R_{my})	104 Ω.cm^2	$(1.3)^{-1}$	25	Blight (1985) †

† Value deduced from reference(s) and then optimised for model. Q_{10} value not from reference, but optimised for model

Discrepancy exists between HH model value and values for human. Value hence optimised for model

†† Values deduced from reference(s) and corrected for concentration and temperature differences

* Considered constant for temperatures between 20 and 42 °C

The internodal conductance (g_{int}) was given by

$$g_{int}(T) = \frac{1}{(N_{my} R_{my}(T)) + R_{mem}(T)} \qquad \left[mS/cm^2\right], \tag{4.8}$$

with R_{my} the temperature-dependent myelin membrane resistance and R_{mem} the temperature-dependent axolemmal membrane resistance (Table 4.2 and Blight, 1985). The assumption of a constant membrane conductance, in which the ionic membrane currents under the myelin sheath are ignored, renders the internodal current (I_{int}) constant (Rattay *et al.*, 2001b). I_{int} was therefore given by

$$I_{int}(T) = g_{int}(T)\, V \qquad \left[\mu A/cm^2\right]. \tag{4.9}$$

Similar to Wesselink *et al.* (1999) the electrical parameters of the nerve fibre cable model were recalculated as values per unit area and optimised for a fibre diameter of 15.0 μm. Electrical parameter values are listed in Table 4.2. The membrane capacitance ($C_{m,n}$) and axoplasmic resistance (R_n) of the nth compartment are defined in Equation 4.1. R_n is a function of the axoplasmic resistivity (ρ_{ax}) and the AP's conduction velocity (v_c) is influenced by ρ_{ax} (Moore *et al.*, 1978; Frijns *et al.*, 1994). Human peripheral sensory nerve fibres can be classified into groups according to conduction velocity and fibre diameter (Schalow, Zäch and Warzok, 1995). Schalow *et al.* (1995) determined v_c values of about 64.0 m.s^{-1} for fibres having a diameter of 15.0 μm and about 10.0 m.s^{-1} for 3.0 – 4.0 μm diameter fibres around 37 °C. Frijns *et al.* (1994) argued that although ρ_{ax} had not been reliably measured before, their model studies suggest a value of 0.07 kΩ.cm at 37 °C and a Q_{10} factor of $(1.3)^{-1}$. For the present human nerve fibre cable model a value of 0.025 kΩ.cm at 37 °C for ρ_{ax} and a corresponding Q_{10} factor of $(1.35)^{-1}$ were selected to give a v_c of 58.3 m.s^{-1} at 37 °C for the 15.0 μm diameter axonal fibre.

Wesselink *et al.* (1999) assumed a fibre diameter of 15.0 μm and a nodal area of 50 μm^2. This results in a nodal length of 1.061 μm, which falls well within the range of 0.88 – 1.25 μm for different nerve fibres (Chiu, Zhou, Zhang and Messing, 1999; Vabnick, Trimmer, Schwarz, Levinson, Risal and Shrager, 1999; Caldwell, Schaller, Lasher, Peles and Levinson, 2000; Waxman, 2000; Scherer and Arroyo, 2002). SEM photographs from these studies, as well as morphometric studies on human sensory nerve fibres (Behse, 1990), indicate that for internodes the axonal to fibre diameter ratio (g-ratio) varies from 0.57 to 0.7. On average smaller g-ratios are associated

with thinner fibres. It appeared that for fibres thicker than 0.34 μm the internodal axolemmal diameter (d_a) varied linearly with the fibre diameter (d_f)

$$d_a = 0.63 d_f - 3.4 \times 10^{-5} \quad [cm]\,. \tag{4.10}$$

The relationship between d_f and the internodal length (L_{int})

$$L_{int} = 7.9 \times 10^{-2} \ln\left(\frac{d_f}{3.4 \times 10^{-4}}\right) \quad [cm]\,, \tag{4.11}$$

however, was only valid for fibre diameters larger than 3.4 μm (Wesselink *et al.*, 1999). Also apparent from the same SEM photographs is the strangulation of the Ranvier node (Chiu *et al.*, 1999; Vabnick *et al.*, 1999; Caldwell *et al.*, 2000; Waxman, 2000; Scherer and Arroyo, 2002). Nodal diameter data from these SEM photographs were plotted against their corresponding d_f values, which ranged from 6.29 μm to 12.0 μm, and a curve fitted through the data points in Matlab. The best fit for the nodal diameter (d_{node}) was a third order polynomial

$$d_{node} = 8.502{\times}10^{5}\,(d_f)^3 - 1.376{\times}10^{3}\,(d_f)^2 + 8.202{\times}10^{-1} d_f - 3.622{\times}10^{-5} \quad [cm]\,, \tag{4.12}$$

and this was confirmed by fitting the curve in Sigmaplot using a different fitting procedure.

4.2.2 Model output calculations

All calculations were performed in Matlab. Differential equations were too stiff to be solved using the ode45 and ode23t numerical solvers, and hence the ode15s solver was used. Modelled nerve fibres ranged from 5.0 – 15.0 μm in diameter and were externally stimulated using a monopolar external electrode placed 1.0 cm from the nerve fibre central axis. The external environment was considered infinite, isotropic and homogeneous with an external resistivity (ρ_e) of 0.3 kΩ.cm at 37 °C (Frijns *et al.*, 1994). External stimulation was thus considered purely resistive and given by

$$V_e = \frac{\rho_e I_{stim}}{4\pi r_{dist}} \quad [mV]\,, \tag{4.13}$$

with r_{dist} the distance between the node and the electrode.

Action potential (AP) characteristics include amplitude, rise and fall times, strength-duration behaviour, refractory period and conduction velocity. Rise and fall times were calculated using the same method as described in Section 3.2.2, where the AP is approximated by a triangle, with the apex at the maximum amplitude (Frijns and ten Kate, 1994). The rising edge intersects the action potential curve at 10% of the maximum amplitude and the rise time is calculated as the time difference between this intersection point and the apex. The falling time is calculated in the same manner using the falling edge.

Strength-duration behaviour is characterised by the rheobase current and chronaxie time. Stimulation pulses were monophasic-anodic and ranged from 0.2 – 2.0 ms in duration. Even though the external stimulation was considered purely resistive, at temperatures lower than 30 °C the strength-duration curves for stimulation pulses up to 1.0 ms could not be fitted with the Weiss linear relationship (Weiss, 1901; Bostock, 1983; Wesselink *et al.*, 1999). Strength-duration curves were thus fitted with the exponential relationship of Lapicque (1907)

$$I_{th} = I_{rb} / \left(1 - e^{-t/\tau_{sd}}\right), \tag{4.14}$$

with I_{th} the threshold current (μA), t the pulse duration (μs), I_{rb} the rheobase current (μA) and τ_{sd} the strength-duration time constant (μs). The chronaxie time (τ_{ch}) is the strength-duration time constant at twice I_{rb}.

Absolute (ARP) and relative (RRP) refractory periods characterise nerve fibre refractory behaviour. Initial nerve fibre stimulation was effected with a 0.1 ms monophasic pulse with amplitude 20% above I_{th}. Stimulation with a second 0.1 ms monophasic pulse resulted in a second propagating AP. The absolute refractory period was defined as the maximum interval between the two pulses in which no second pulse, with amplitude of up to 400% I_{th}, could be elicited. The relative refractory period was the minimum interval between the two pulses in which an impulse of at most 101% I_{th} was required to elicit the second pulse (Wesselink *et al.*, 1999).

4.3 RESULTS

A general human peripheral sensory nerve fibre having diameters in the range of 5.0 – 15.0 μm was simulated in Matlab and externally stimulated with a monopolar electrode. Stimulation pulses were square, monophasic-anodic and only single pulses were used.

4.3.1 Action potential rise and fall times

AP rise and fall times were calculated in the temperature range of 20 – 37 °C. Figure 4.2 shows an example of a propagating AP for a 15.0 μm fibre calculated at 20 °C. Rise and fall times for a 15.0 μm fibre are compared to experimentally estimated results (Table 4.3). Rise times were less than 0.5% shorter than the estimated results at 20 and 25 °C, while being 4.2% shorter at 37 °C. The rise time decreased by 24.5% (Q_{10} factor of $(1.76)^{-1}$) from 20 to 25 °C.

Table 4.3: Simulated rise and fall times for a 15.0 μm diameter general human peripheral sensory nerve fibre cable model compared to experimentally estimated results from human peripheral nerve fibres.

Parameter	**Specifications**	**Value**		
	(15.0 μm fibre diameter)	**Human peripheral nerve fibre model**	**Experimental results**	**Reference**
Rise time (μs)	20 °C	269	270	Schwarz *et al.* (1995)
	25 °C	203	204	Schwarz *et al.* (1995)
	37 °C	115	120	Wesselink *et al.* (1999)
Fall time (μs)	20 °C	1840	1829	Schwarz *et al.* (1995)
	25 °C	1424	1464	Schwarz *et al.* (1995)
	37 °C	754	470	Wesselink *et al.* (1999)

Fall times were 6% longer at 20°C and 2.7% shorter at 25 °C than the estimated results, while being 60% longer at 37 °C. Compared to the results of the Ranvier node model (Section 3.3) the fall time decreased by 22.6% (Q_{10} factor of $(1.66)^{-1}$) from 20 to 25 °C, which was steeper than the 20% decrease of the experimental results. Calculated rise and fall times, and hence AP duration, varied with fibre diameter (Figure 4.3).

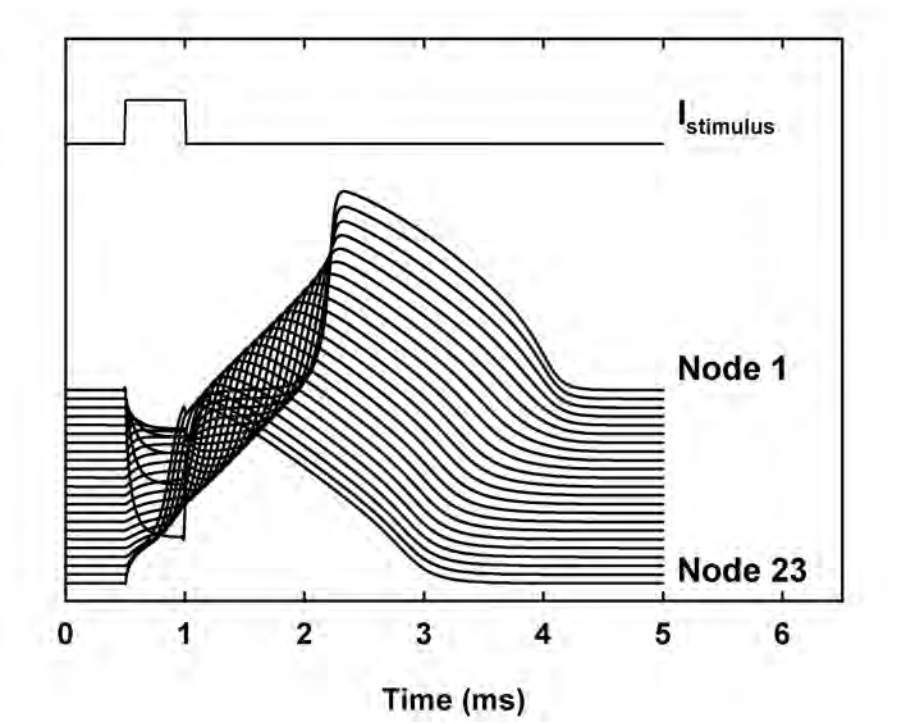

Figure 4.2: Propagating AP for a 15.0 μm fibre plotted at 20 °C. The fibre was externally stimulated with a monopolar electrode. The stimulating pulse was square, monophasic and anodic and 0.5 ms in duration. Only nodal APs are shown. Internodal APs were similar in nature than nodal APs.

In general, independent of temperature, rise times increased with a decrease in fibre diameter down to 7.5 μm (Figure 4.3(a)). However, below 7.5 μm rise times decreased again, with the rise time of a 5.0 μm diameter fibre similar to the rise time of a 12.5 μm diameter fibre.

Fall times decreased between 15.0 μm and 10.0 μm and then increased again for smaller fibre diameters, with the fall time of a 5.0 μm diameter fibre being similar to the fall time of a 15.0 μm diameter fibre (Figure 4.3(b)). The relationships between rise or fall times and fibre diameter became more pronounced as the temperature was decreased from body temperature. So, for example, the slopes of the fall time curve at 25 °C were more than twice as steep as the corresponding curve slopes at 37 °C (Figure 4.3(b)).

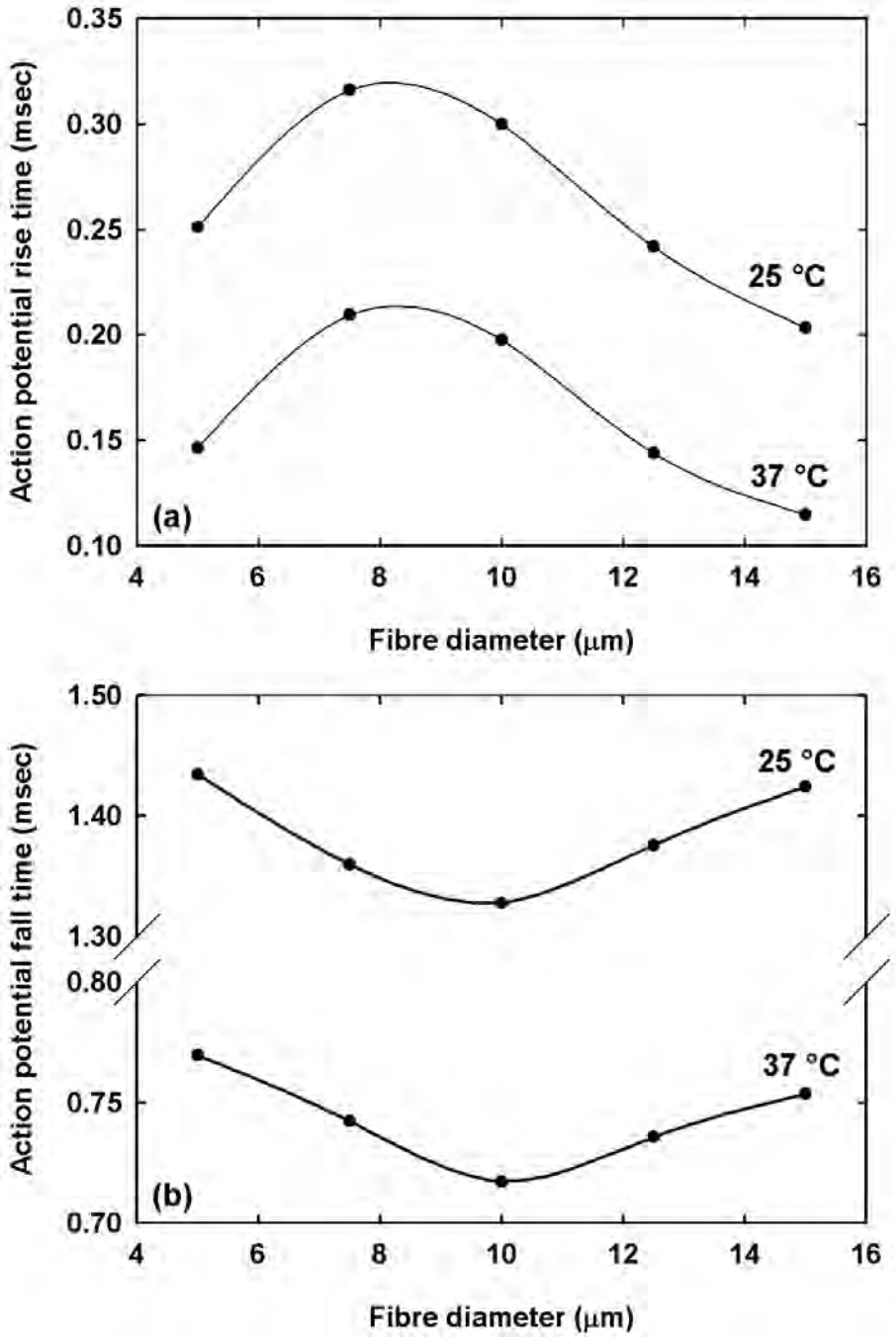

Figure 4.3: Relationship between AP rise and fall times and fibre diameter plotted at 25 °C and 37 °C. (a) AP rise times became longer with a decrease in temperature and increased with a decrease in fibre diameter down to 7.5 μm. (b) AP fall times were longer at lower temperatures compared to higher temperatures. Fall times decreased with a decrease in fibre diameter down to 10.0 μm and increased for thinner fibres.

4.3.2 Action potential duration times

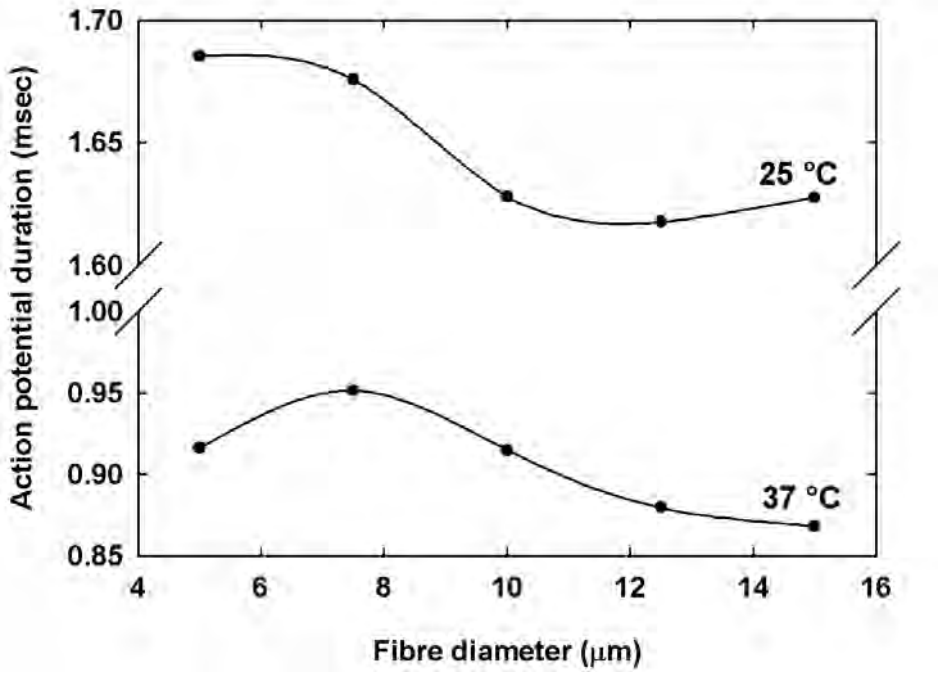

Figure 4.4: AP duration plotted against fibre diameter. For fibre diameters larger than 7.5 μm, AP duration showed an inverse relationship to fibre diameter at temperatures higher than 27 °C. At lower temperatures durations increased again for fibres larger than 12.5 μm.

The AP duration is the sum of the rise and fall times. AP duration, for fibre diameters larger than 7.5 μm, followed the trend of an inverse relationship to the fibre diameter (Paintal, 1966) at temperatures higher than 27 °C (Figure 4.4). At lower temperatures this relationship did not hold for fibre diameters larger than or equal to 12.5 μm.

Normalising these relationships to their respective values at 37 °C indicated a slightly steeper increase in AP duration in the thicker fibres with a decrease in temperature, compared to the thinner fibres; the average Q_{10} factor being about $(1.65)^{-1}$ (Figure 4.5). The curve of the 5.0 μm diameter fibre was similar to the 12.5 μm diameter curve and was thus omitted.

The change in slope around 27 °C for all fibre thicknesses is not apparent from Figure 4.5. For fibres thicker than 7.5 μm, the slopes increased by about 5.6% in the temperature range above 27 °C, compared to the less steep slope of about 3% in the

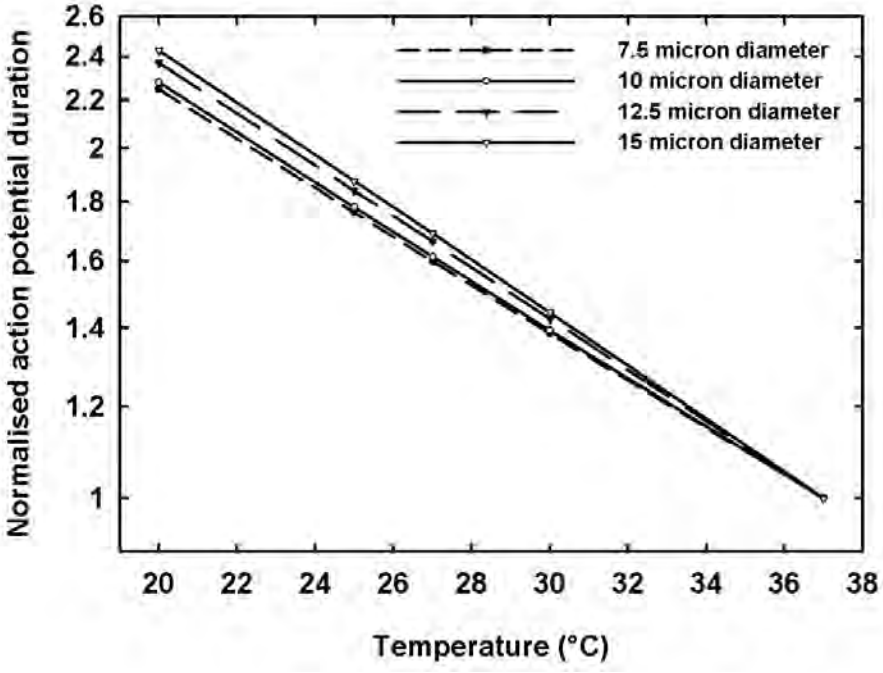

Figure 4.5: Temperature dependence of normalised AP durations plotted for fibre diameters larger than 7.5 μm. These results were obtained from curves similar to and including the curves in Figures 4.3 and 4.4. Results were normalised at AP durations at 37 °C. Curve slopes indicated a faster increase in AP duration for thicker fibres.

temperature range below 27 °C (Figure 4.6).

4.3.3 Action potential amplitude

Calculated amplitudes followed the trend of an amplitude decrease with temperature increase (Buchthal and Rosenfalck, 1966; Schwarz and Eikhof, 1987; Frijns *et al.*, 1994; Wesselink *et al.*, 1999). For the 15.0 μm fibre amplitudes around 115 mV were obtained at 20 and 25 °C and decreased by less than 1% between 20 and 25 °C. At 37 °C an amplitude around 112 mV was obtained. Amplitudes at corresponding temperatures decreased with a decrease in fibre diameter, but all amplitudes were larger than 100 mV. The exception to this trend again was the 5.0 μm fibre with amplitudes comparable to those of the 12.5 μm fibre.

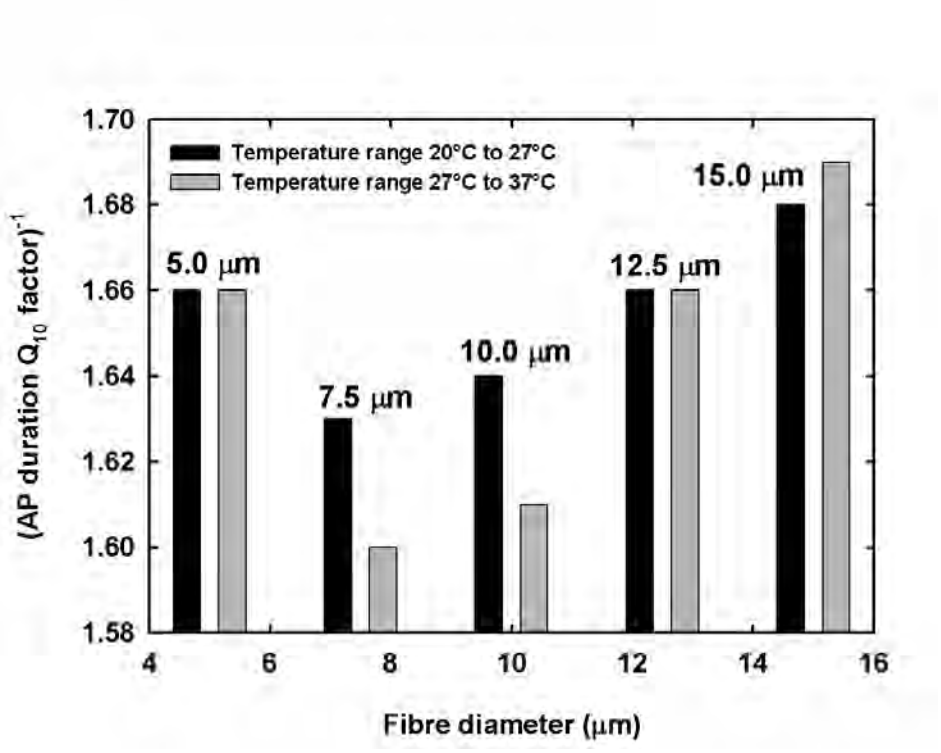

Figure 4.6: AP duration Q_{10} factors for temperature ranges 20 to 27 °C and 27 to 37 °C respectively, plotted against fibre diameter. Q_{10} factors were calculated from the curves in Figure 4.5. For fibre diameters larger than 7.5 μm, Q_{10} factors of the higher temperature range increased faster with a fibre diameter increase compared to the lower temperature range, indicating a change in AP duration slope in all fibres at 27 °C.

4.3.4 Conduction velocities

Conduction velocity (v_c) values of the new human nerve fibre cable model exhibited fibre diameter dependency (Figure 4.7), as well as temperature dependency (Table 4.4).

For fibre diameters thicker than 12.5 μm, v_c values compared well with the values measured by Schalow *et al.* (1995), but for thinner fibres v_c values were underestimated. Conduction velocities per diameter varied from 2.9 – 3.5 s^{-1} for fibre diameters ranging from 5.0 – 15.0 μm at 37 °C. Lowitzsch *et al.* (1977) measured average v_c values for human ulnar nerve sensory nerve fibres. Comparison to the data of Schalow *et al.* (1995) suggests an average ulnar fibre diameter of about 13.0 μm. Hence the v_c temperature dependency of a 13.0 μm simulated nerve fibre is compared to the results achieved by Lowitzsch *et al.* (1977) (Table 4.4). Simulated v_c values decreased with

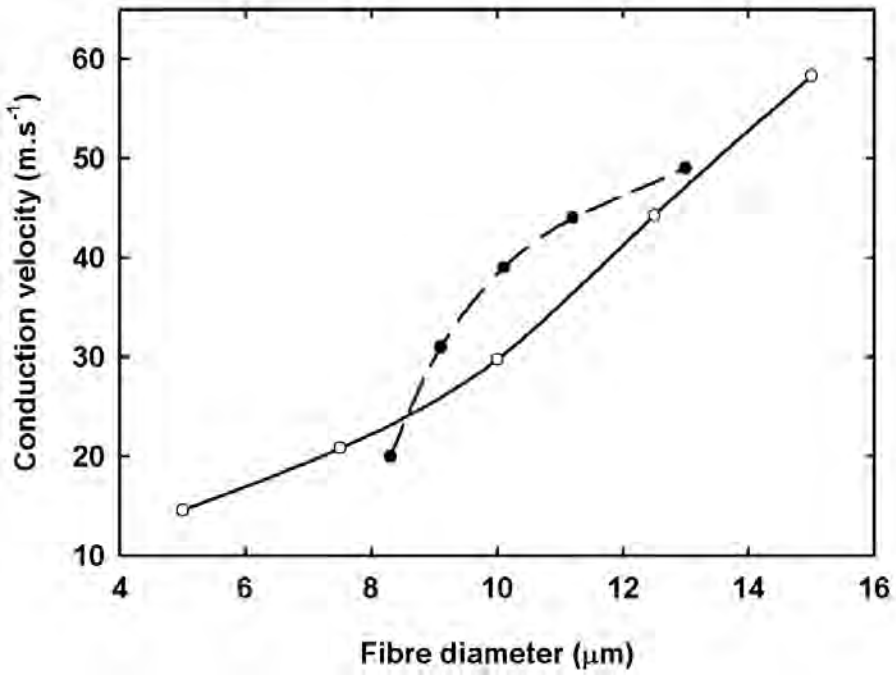

Figure 4.7: Conduction velocity plotted against fibre diameter (continuous line; open circles). Simulations were performed at 37 °C. Experimental data from Schalow *et al.* (1995) (dashed line; closed circles).

Table 4.4: Simulated temperature dependency of conduction velocity, ARP and RRP and chronaxie times for a general human peripheral sensory nerve fibre of about 13.0 μm diameter. Experimentally estimated results from Lowitzsch *et al.* (1977) are indicated in parenthesis for comparison.

Parameter	**Temperature (°C)**				**Q_{10} value**		**Reference**
	20	**25**	**30**	**35**	**30 – 20**	**35 – 25**	
Conduction velocity ($m.s^{-1}$)	28.81 (29.65)	36.52 (36.18)	42.35 (42.72)	46.20 (49.26)	1.47 (1.44)	1.27 (1.36)	Lowitzsch *et al.* (1977)
ARP (ms)	2.30 (3.07)	1.70 (1.72)	1.30 (1.02)	1.00 (0.54)	$(1.77)^{-1}$ $((3.01)^{-1})$	$(1.70)^{-1}$ $((3.18)^{-1})$	Lowitzsch *et al.* (1977)
RRP (ms)	20.40 (20.09)	10.30 (10.23)	5.10 (5.76)	3.16 (3.19)	$(4.00)^{-1}$ $((3.49)^{-1})$	$(3.23)^{-1}$ $((3.21)^{-1})$	Lowitzsch *et al.* (1977)
Chronaxie (μs)	737.4	439.9	245.1	138.4 (37 °C)	$(3.01)^{-1}$	$(2.62)^{-1}$	

increased temperature, but at a slower rate compared to real nerve fibre data. The maximum simulated value of 46.20 $m.s^{-1}$ at 35 °C was 6.2% lower than the experimentally measured value. Similar to the experimental results, the Q_{10} factors were different for the temperature ranges 20 – 30 °C (Q_{10} factor of 1.47) and 25 – 35 °C (Q_{10} factor of 1.27).

4.3.5 Refractory periods

ARP and RRP of the 13.0 μm simulated nerve fibre is compared to the results (Table 4.4) obtained by Lowitzsch *et al.* (1977). At body temperature (37 °C) the ARP was 0.9 ms and the RRP 3.05 ms. Both ARP and RRP decreased with an increase in temperature. Q_{10} factors indicated that the decrease was more pronounced in the lower temperature range of 20 – 30 °C than in the higher range of 25 – 35 °C, similar to the trend observed experimentally. For RRP the calculated rates overestimated the experimentally estimated rates by less than 15.0%. However, the calculated ARP results underestimated the experimental rates by more than 40%. Simulated ARP values did not vary significantly for fibres thicker than 10.0 μm, but increased by about 30% when the fibre diameter was decreased to 5.0 μm.

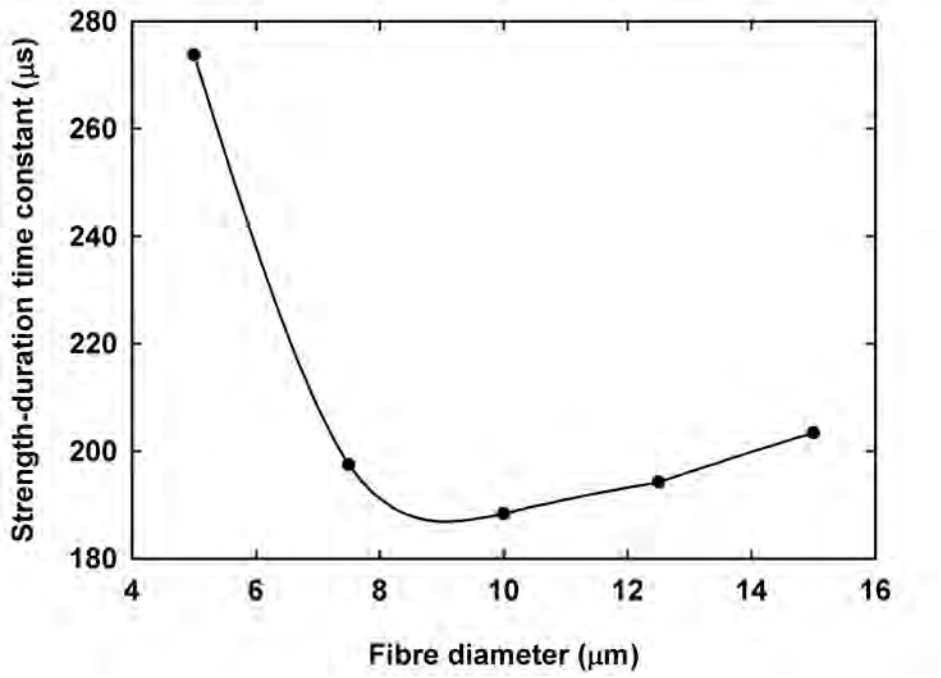

Figure 4.8: Strength-duration time constant plotted against fibre diameter. Simulation temperature was 37 °C.

4.3.6 Strength-duration relationships

Strength-duration curves were calculated for nerve fibres in the range of 5.0 – 15.0 μm. Stimulation was performed with a single monopolar external electrode placed 1.0 cm from the nerve fibre central axis. Stimulation pulses were monophasic-anodic and ranged from 0.2 – 2.0 ms in duration. The strength-duration time constant (τ_{sd}) showed nerve fibre diameter dependence (Figure 4.8), ranging from 184.3 μs to 273.6 μs at 37 °C over the studied nerve fibre diameter range. However, unlike the results obtained by Wesselink *et al.* (1999), τ_{sd} values did not decrease monotonically with increased fibre diameter, but increased again for fibre diameters larger than 10.0 μm. Chronaxie times (τ_{ch}) were about 30.5% lower than τ_{sd} values for all fibre diameters. Rheobase current was increased by 51.0% by increasing the fibre diameter from 5.0 μm to 10.0 μm and decreased by 11.6% for a further diameter increase to 15.0 μm.

Strength-duration relationships were calculated at temperatures between 20 and 37 °C

with τ_{ch} values showing an inverse relation to temperature (Table 4.4). This relationship was non-linear, with a larger rate of increase in τ_{ch} values for the temperature range 20 – 30 °C (Q_{10} factor of $(3.01)^{-1}$) compared to the range 25 – 37 °C (Q_{10} factor of $(2.62)^{-1}$), as calculated for a fibre of diameter 13.0 μm. The same trend was evident for the other fibre diameters as well.

4.4 DISCUSSION

In this chapter a new generalised human peripheral sensory nerve fibre cable model was developed. The nerve fibre model was based on the cable model by Rattay *et al.* (2001b), but modified to a simple double cable structure based on the model of Blight (1985). Modelled Ranvier nodes utilised the human Ranvier node model dynamics described in Chapter 3. The temperature dependence of all parameters was included.

Single-cable nerve fibre models include a small fast potassium (I_{Kf}) current, but since the myelin is considered a near perfect insulator with high resistance, the modelled nodes have to set their own resting potential (see for example the human nerve fibre models by Schwarz *et al.*, 1995; Wesselink *et al.*, 1999). This is effected through the inclusion of a high conductance leakage current (I_L), mostly carried by K^+ (Baker, 2002). In this human nerve fibre model the extracellular to intracellular ion concentration ratios for the I_L and I_K currents were similar, suggesting that I_L was mostly carried by K^+ (see the discussion in Section 3.4). However, in this model the myelin was not considered a near perfect insulator, resulting in smaller g_L values than the values used in the existing human nerve fibre models.

Paintal (1966) demonstrated an inverse relationship between AP duration and conduction velocity in cat sensory nerve fibres. AP duration also varies inversely with temperature in both slow and fast conducting fibres, although the slopes of these curves change at 27 °C. In slow conduction fibres the slopes are almost the same for the temperature ranges below and above 27 °C respectively, having Q_{10} factors around $(3.1)^{-1}$ below 27 °C and $(3.4)^{-1}$ above 27 °C (refer to Figure 4 in Paintal, 1966). The slopes for fast and slow conducting fibres are almost the same for temperatures above 27 °C. However, for temperatures below 27 °C, the slopes become levelled off in the faster fibres, having a Q_{10} factor of about $(2.27)^{-1}$ for a 64 m.s^{-1} fibre. This constitutes a

26.7% decrease in slope between slow and fast fibres.

In the human sensory nerve fibre model the inverse relationship between AP duration and fibre thickness, i.e. conduction velocity, held for simulated fibres thicker than 7.5 μm. AP duration varied inversely with temperature, but with the average Q_{10} factor for the slopes only being only about $(1.65)^{-1}$, compared to the value of $(3.4)^{-1}$ for the results obtained by Paintal (1966). Similar to the results of Paintal (1966), the curve slopes changed around 27 °C, but became steeper instead of flatter (see Figure 4.6). However, when the increase in slope steepness with increased fibre thickness for the temperature range below 27 °C was compared with the slope steepness increase for the temperature range above 27 °C, the former increased by about 3.0% compared to the 5.3% of the latter. In the thicker fibres the overall slope also changed less than 1% between the two temperature ranges, compared to a change of about 1.8% in the thinner fibres. It therefore seemed that the modelled human nerve fibres displayed the same trend of levelled off slopes in thicker (i.e. faster) fibres for temperatures below 27 °C, albeit a factor 10 less than for fibres in the Paintal (1966) study.

Schalow *et al.* (1995) determined that the ratio of the conduction velocity (v_c) to fibre diameter in afferent sensory nerve fibres ranges between 2.5 μs^{-1} and 4.1 μs^{-1}. In the model by Wesselink *et al.* (1999), the ratio varies between 3.1 μs^{-1} and 4.3 μs^{-1} for fibre diameters in the range of 5.0 – 15.0 μm at 37 °C. In the present human sensory nerve fibre model the simulated conduction velocity to fibre diameter ratios compare favourably with these results. However, v_c values were underestimated compared to the results of Schalow *et al.* (1995) and Wesselink *et al.* (1999) and did not display the linear relation to fibre diameter as the results of Wesselink *et al.* (1999) did. An analysis of the sensitivity of the v_c to model parameters suggested that v_c values were most sensitive to the internodal length and, to a lesser degree, the axoplasmic resistivity (ρ_{ax}) (unpublished results). For the present human nerve fibre cable model the values for ρ_{ax} and corresponding Q_{10} factor were selected to give a v_c of 58.3 m.s^{-1} at 37 °C for the 15.0 μm diameter axonal fibre. However, the same analysis study suggested different ρ_{ax} values when the internodal length for the 15.0 μm diameter fibre was varied. This added an additional degree of freedom to the optimisation procedure and would have required optimisation not only for a 15.0 μm diameter fibre, but also for fibres of different diameters. Owing to the lack of sufficient parameter data for fibres other than the 15.0 μm diameter fibre, it was assumed that it would be feasible to use the same relationship between fibre diameter and internodal length as

Wesselink *et al.* (1999). This resulted in the present model having the same internodal lengths as the model of Wesselink *et al.* (1999), but with a smaller ρ_{ax} value. Hence this difference might account for the underestimated v_c values simulated for thinner nerve fibres.

The calculated ARP of about 0.9 ms at 37 °C was longer than the experimentally estimated range of 0.58 – 0.79 ms for humans (refer to Table 1 in Wesselink *et al.*, 1999). The relation between ARP and fibre diameter was similar to the findings of Paintal (1965), who found that in cat nerve fibres, ARP values in faster (i.e. thicker) fibres varied insignificantly, but they varied inversely to v_c in slower fibres. Calculated RRP of 3.05 ms compared favourably with experimental results of about 3.0 ms at 37 °C (Lowitzsch *et al.*, 1977; Wesselink *et al.*, 1999).

Strength-duration behaviour indicated fibre diameter dependency, but unlike the model of Wesselink *et al.* (1999), rheobase current, strength-duration time constants and hence also chronaxie times did not decrease monotonically with a fibre diameter increase. Chronaxie times where shorter than experimentally estimated times (refer to Table 1 in Wesselink *et al.*, 1999). However, it must be remembered that the experimental values were estimated from compound fibre data (see for example studies by Kiernan *et al.*, 2001; Burke *et al.*, 1999), in contrast to the single fibre data presented here. Even so the chronaxie times compared favourably with times ranging from 113 – 202 μs from the Wesselink *et al.* (1999) model.

Different experimental studies on the effect of temperature on the chronaxie times in human cutaneous afferent nerve fibres show that chronaxie times do not vary significantly with a change in temperature (Mogyoros, Kiernan and Burke, 1996; Burke *et al.*, 1999; Kiernan *et al.*, 2001). Simulated results from the new human nerve fibre model were in contrast to these findings, showing an increase of more than a factor 5 for a decrease in temperature from 37 to 20 °C (see Table 4.4). Bostock (1983) suggested that the linear relationship of Weiss (1901) best estimates chronaxie times in simulated myelinated nerve fibres. Mogyoros *et al.* (1996) confirmed this finding for experimentally estimated chronaxie times in compound fibre data. Strength-duration curves at temperatures below 30 °C for single human nerve fibres modelled in the present study could not be fitted with the Weiss relationship, and were hence fitted with the exponential relationship of Lapicque (1907). As the temperature was increased from 20 °C, exponential fitting became less accurate; suggesting that a hy-

perbolic fit might be more accurate. This difference in strength-duration behaviour with temperature was not observed in previous human nerve fibre studies (compare Wesselink *et al.*, 1999), and needs further in-depth investigation.

Parameter data used in the present human sensory nerve fibre model were determined from published data from various studies of human nerve fibres. As mentioned in Section 4.2, Frijns *et al.* (1994) argued that ρ_{ax} had not been reliably measured before. Wesselink *et al.* (1999) derived their fibre-diameter-to-internodal-length relation from published data by Behse (1990). The third order polynomial relationship between nodal diameter and fibre diameter was determined by curve fitting to data derived from SEM photographs. Even though the size estimation of myelinated peripheral nerve fibres is commonly performed in quantitative neuromorphology, Geuna, Tos, Guglielmone, Battiston and Giacobini-Robecchi (2001) cautioned that the different methodologies used in such studies may bias the results. Newer computer-automated measurement approaches are more efficient and have a higher accuracy than older manual methods (Geuna *et al.*, 2001). However, the data that were available to determine the model parameter values did come from older studies and parameter values might be different from the true values for *in vivo* nerve fibres. Since the strength-duration properties of a nerve fibre depend on nodal membrane properties (Bostock, 1983), such differences might account for the discrepancy found in chronaxie values; for both temperature and fibre diameter variations.

Furthermore, the temperature dependency of a large proportion of the parameters was effected through the use of Q_{10} factors, in view of a lack of temperature-dependent studies done on individual human nerve fibre parameters. The use of Q_{10} factors assumed a linear relation between the parameter values and temperature variation. Temperature dependency results from this study suggested the assumption of such linear relationships over the entire temperature range from 20 – 37 °C might not be valid.

Lastly, mention must be made of the differences observed in the thinner, especially the 5.0 μm, nerve fibres compared to the thicker nerve fibres. Part of these behaviour differences might be explained by the above-mentioned discussion. However, the membrane parameters of the general nerve fibre were, in accordance with the previous modelling work by Schwarz *et al.* (1995) and Wesselink *et al.* (1999), developed and optimised for a 15.0 μm fibre and then 'scaled down' to model thinner fibres. Para-

meters used in the human Ranvier node model were based on values determined from studies done on thicker sensory nerve fibres (Section 3.2) and these parameter values may be different in thinner fibres. So for example, the slow potassium current at the Ranvier node is mediated by different KCNQ channels (Taylor *et al.*, 1992; Devaux *et al.*, 2004; Schwarz *et al.*, 2006). Ranvier nodes in thinner fibres showed labelling for KCNQ2 and KCNQ3, while nodes in thicker fibres showed labelling only for KCNQ2 (Schwarz *et al.*, 2006).

4.5 CONCLUSION

The objective of this study was to determine if the recently developed human Ranvier node model, which is based on a modified version of the HH model, could predict the excitability behaviour in human peripheral sensory nerve fibres. Up to now the most physiologically and morphometrically correct nerve fibre models describing these behaviour in humans are based on the Goldman-Hodgkin-Katz (GHK) current and voltage equations (Schwarz *et al.*, 1995; Wesselink *et al.*, 1999). These equations are more complex than the HH model equations used in the present model and are used to replace the linear current-voltage relationships of the opening and closing of the sodium and potassium channels in the HH model with non-linear relationships found in vertebrate excitable cells (Hille, 2001). This study was the first to show that the HH model equations could successfully be modified to predict excitability behaviour in humans without using the GHK equations.

Furthermore, temperature dependence of all parameters over the temperature range of 20 to 37 °C was addressed. The human nodal model was incorporated into a simple double cable nerve fibre model and simulation predictions compared favourably with experimentally determined results. However, as in the case of the single human Ranvier node model, chronaxie times were overestimated at temperatures lower than body temperature. This can be attributed to shortcomings in the fitting procedure employed to determine the chronaxie times, the bias in measured parameter values due to the measuring methodologies used, as well as the possible incorrect assumption of linear parameter relationships to temperature variation. Further study in this regard is advised.

In the last phase of the development of the human ANF model this general sensory nerve fibre model will be incorporated into the existing ANF model by Rattay *et al.* (2001b). This will be the topic of the next chapter.